IEEE Access
Multidisciplinary | Rapid Review | Open Access Journal

Received December 6, 2021, accepted December 17, 2021, date of publication December 27, 2021, date of current version January 6, 2022.

Digital Object Identifier 10.1109/ACCESS.2021.3138963

Electron-Optic System With High Compression of a Multiple Elliptic Electron Beam for a Miniaturized THz-Band Vacuum Electron Device

IGOR A. NAVROTSKY[1,3] AND NIKITA M. RYSKIN[1,2], (Senior Member, IEEE)
[1]Saratov Branch, Kotelnikov Institute of Radio Engineering and Electronics, 410019 Saratov, Russia
[2]Institute of Physics, Saratov State University, 410012 Saratov, Russia
[3]Fundamental Research Laboratory, RPE "Almaz," 410033 Saratov, Russia

Corresponding author: Nikita M. Ryskin (ryskinnm@info.sgu.ru)

This work was supported in part by the Russian Science Foundation under Grant 17-12-01160.

ABSTRACT Electron-optic systems (EOSs) with high compression are required for THz-band vacuum-tube electron devices to reduce the cathode load, which is necessary to increase lifetime and enable operation in a continuous-wave (CW) mode. However, it is difficult to achieve high compression of multiple electron beams. In this article, we present the design and simulation of EOS with triple elliptic electron beam for a 0.2-THz traveling-wave tube. The triode electron gun with planar electrodes provides 3×0.06-A electron beam with compression factor of 16. At the cathode, the current density is 26.31 A/cm^2 while in the beam tunnel it is higher than 400 A/cm^2. The magnetic focusing system with 1.34-T axial magnetic field consisting of Nd–Fe–B permanent magnets and pole pieces is also designed. The numerical simulation predicts stable beam transmission at 25-mm distance.

INDEX TERMS Electron gun, electron-optic system, multiple electron beam, traveling-wave tube.

I. INTRODUCTION

Numerous applications, such as high-data-rate wireless communications, high-resolution radar, and non-destructive evaluation, require miniaturized high-power wideband sources of coherent terahertz (THz) radiation. Therefore, increasing power of THz-band microfabricated vacuum electron devices (μVEDs) is an important problem. The main issue in the development of μVEDs is the need for an ultrahigh-current-density electron beam. Using sheet or multiple electron beam may be a promising solution [1]. Several designs of μVEDs with multiple sheet electron beam interacting with a high-order transversal mode of an overmoded slow-wave structure (SWS) have been suggested [2]–[8]. It is expected that such devices can provide over 100 W output power at sub-THz frequencies.

Nevertheless, these devices require electron beam current density higher than 100 A/cm^2. Therefore, there is a strong need in electron-optic system (EOS) with electron beam compression, which allows reducing of the cathode loading and enables CW operation. Design and development of EOSs with converging sheet electron beams have been reported in several works [9]–[12]. However, in case of multiple beam this technology is still poorly developed.

In [13] and [14], we presented the EOS with 6.5-times compression of triple elliptic electron beam for a 0.2-THz traveling-wave tube (TWT). The triode electron gun with a magnetically shielded cathode has been developed and 3×0.031 A current, i.e., 93-mA total current has been measured. The current density at the cathode was about 19 A/cm^2 while in the beam tunnel it exceeded 120 A/cm^2. The experiment on beam transportation in 0.55-T axial focusing magnetic field showed 60% transmission at 25-mm distance.

In [15], a dual-sheet-beam EOS for a 0.34-THz TWT was designed and studied by 3-D particle-in-cell (PIC) numerical simulation. The EOS produced 2×0.043 A electron beam with 3.3-times compression. Refs. [16]–[18] presented design and simulation of EOSs with compression of a triple cylindrical-shaped electron beam. In [16], the EOS for a 0.22-THz TWT 3×0.1 A beam with 29.24-A/cm^2 cathode loading and compression factor of 10 was reported. In [17] and [18], the EOS for a W-band TWT with even higher 3×0.15 A current and compression factor of 4 was studied. Nevertheless, the required cathode loading was higher than 100 A/cm^2.

The associate editor coordinating the review of this manuscript and approving it for publication was Wenxin Liu.

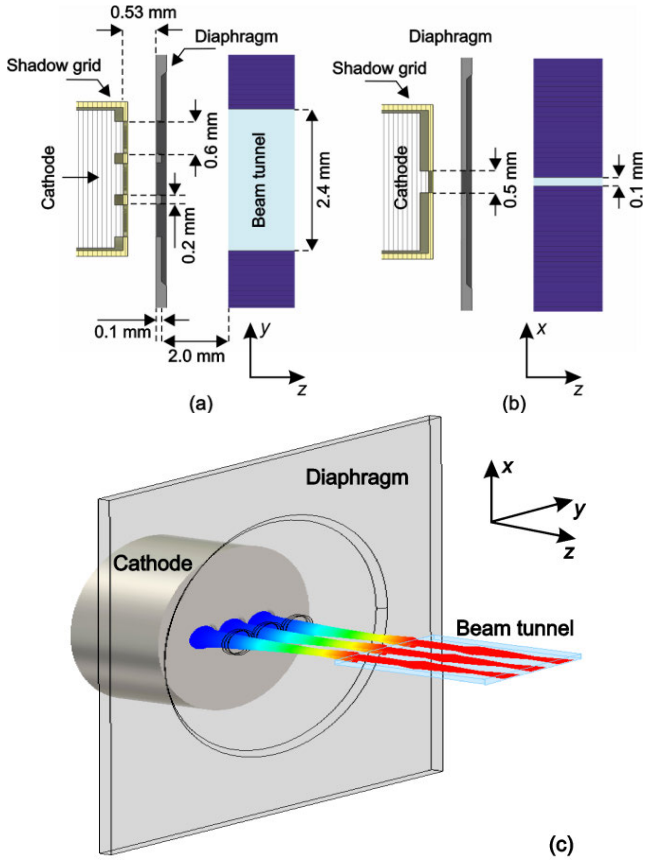

FIGURE 1. Schematic of the electron gun. (a) *y-z* view. (b) *x-z* view. (c) 3-D view.

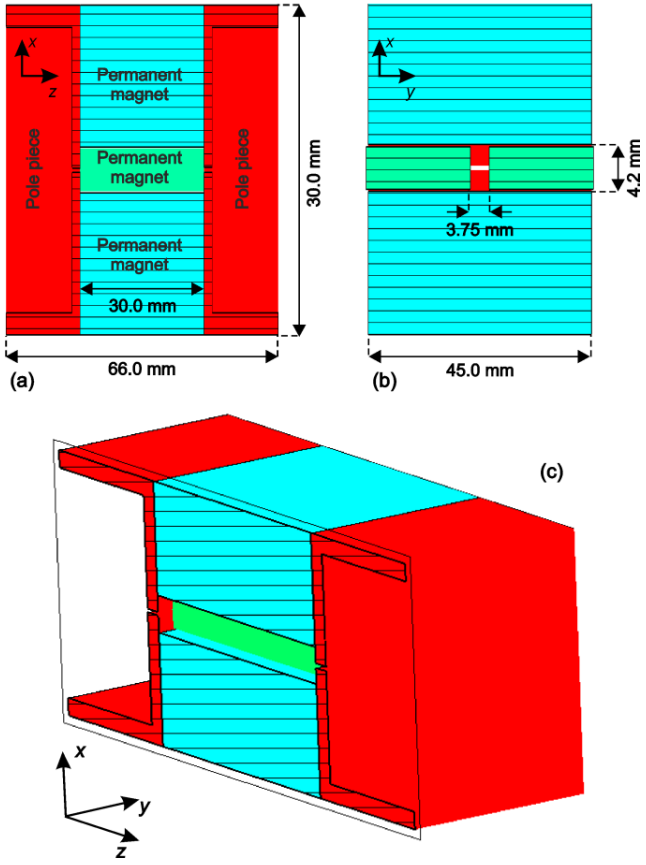

FIGURE 2. Schematic of the magnetic system. (a) *x-z* cutaway view at y = 0. (b) *x-y* cutaway view at z = 17.5 mm. (c) 3-D view.

In this article, we improve the design presented in [13], [14] in order to increase the beam current and to reduce the cathode loading. The new EOS produces a 3 × 0.06 A elliptic-shaped electron beam. High compression factor of 16 is demonstrated in 3-D PIC simulation. The corresponding cathode loading is 26.31 A/cm^2, while the averaged current density of the compressed beam is ∼ 400 A/cm^2.

II. ELECTRON-OPTIC SYSTEM DESIGN

A. ELECTRON GUN

Schematic of the electron gun is presented in Fig. 1. This is a triode-type gun with planar electrodes. The planar shape of the electrodes essentially simplifies the fabrication and assembling process. The gun consists of a cathode, a shadow grid, a focusing electrode (diaphragm) and an anode with a beam tunnel. The cathode is formed by three 0.5 mm × 0.6 mm elliptic-shaped protrusions. The elliptic shape is preferable to circular one because it provides less current interception at the anode. To increase the beam current, vertical dimension of the protrusions was increased in comparison with the gun developed in [13], [14]. Distance of 0.2 mm between the cathodes in *y*-direction has been selected to get 0.8-mm distance between the beamlet axes. This provides effective interaction with the higher-order TE$_{03}$-like mode of the overmoded staggered grating SWS with 2.4-mm beam tunnel width [19], [20].

The focusing diaphragm has three elliptic holes with the same dimensions as the cathode protrusions. This electrode may be used as a control grid serving for beam modulation. The diaphragm thickness is 0.1 mm. However, at the edges the thickness is increased to improve the mechanical strength.

B. MAGNETIC SYSTEM

A strong axial magnetic field B_z is applied for electron beam focusing. In [12], we presented the design of 1.1-T permanent-magnet magnetic focusing system (MFS). In this work, we modified the design of [12] in order to enlarge the axial magnetic field above 1.3 T, which is necessary to achieve high compression. Schematic of the MFS with dimensions is presented in Fig. 2. Since the length of the interaction space of the TWT is assumed as 25 mm, the axial size of the magnets has been set to 30 mm, which is twice less than in [12]. The dimension of the borehole is 4.2 mm × 3.75 mm that is large enough for placing the SWS circuit. The apertures of the pole pieces have 0.5 mm × 12 mm dimension.

In the simulations, the magnetic material is set as $Nd_2Fe_{14}B$ with remanence of 1.48 T. The material for magnetic pole pieces is set as steel-1008 with $\mu = 10^3$.

Fig. 3 shows the plot of axial component of the magnetic field versus axial coordinate z. It demonstrates nearly constant value of the magnetic field $B_z \approx 1.345$ T at 25-mm distance.

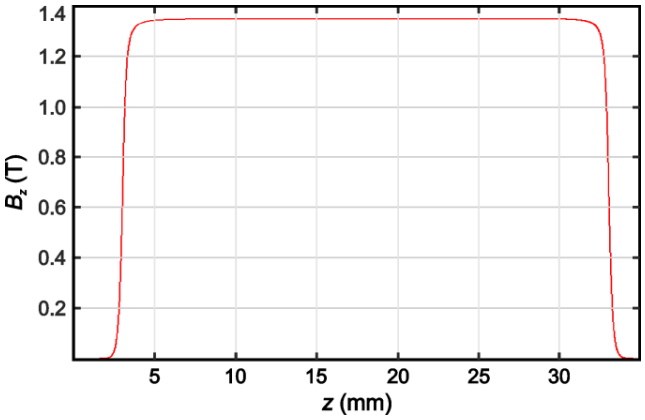

FIGURE 3. Axial profile of the focusing magnetic field.

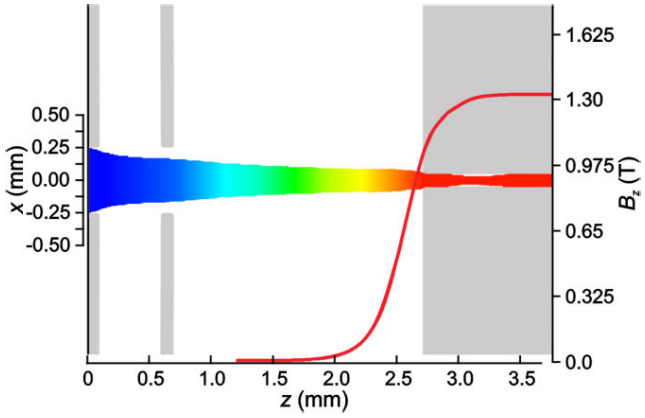

FIGURE 4. *x-z* projection of the electron trajectories and the magnetic field profile.

III. RESULTS AND DISCUSSION

The electron gun is simulated by using the 3-D CST Particle Studio simulator [21]. In the simulations, we set the cathode parameters same as for the M-type dispenser cathode presented in [12]. At the cathode, the electrons are assumed emitted with a spread angle of 5° and with a kinetic energy spread set in accordance with the Maxwell–Boltzmann distribution. The cathode temperature and electron work function are set to 1250°C and 2.055 eV, respectively. The cathode temperature has been slightly increase in comparison with [12] to get higher current.

In Fig. 4, electron trajectories in the midplane $y = 0$ are plotted together with the magnetic field profile. The compressed beam is injected into the 0.1 mm × 2.4 mm beam tunnel. The cathode is magnetically shielded. In this simulation, the anode voltage is set to $V_a = 21.4$ kV, while the voltage at the focusing electrode is $V_g = 1.48$ kV. Fig. 4 shows strong compression of the beam. Despite deposition of some electrons at the anode, the collector current is 180.97 mA while the body current is only 4.91 mA, i.e., the beam transmission is 97.3%.

Fig. 5 shows current-voltage characteristics of the gun. In this figure, the total cathode current I_c, the collector current I_{col}, and the body current I_b are plotted versus the control

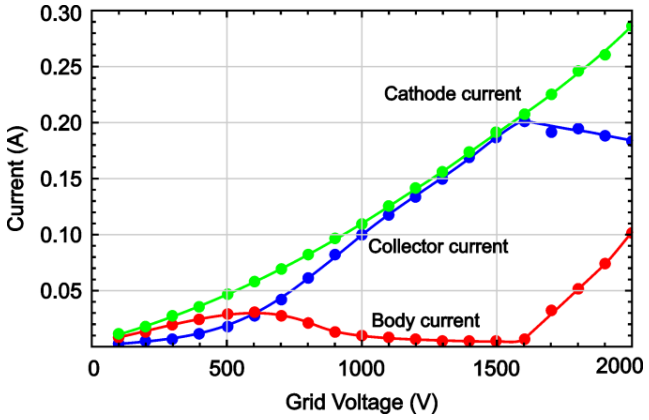

FIGURE 5. Current-voltage characteristics of the electron gun. Cathode current, collector current, and body current versus the control grid voltage are plotted at the anode voltage of 21.4 kV.

grid voltage V_g. The anode voltage is set to 21.4 kV to provide synchronism with the forward wave in the staggered grating slow-wave structure designed in [19], [20]. When the grid voltage is below 1000 V, there is a significant beam interception at the anode. At $V_g = 1.0 - 1.6$ kV, the body current is very small, i.e., good beam focusing is observed. However, when $V_g > 1.6$ kV, beam the body current starts to rapidly increase. Maximal collector current $I_{col} = 0.2$ A is attained at 1.6-kV grid voltage.

This behavior is explained by Fig. 6 where *x-z* current density profiles calculated at different values of the grid voltage are presented. At low grid voltage, overfocusing of the beam takes place, as is shown in Fig. 6(a). The crossover is located well before the anode plane. As a result, most of the beam current is intercepted by the anode. With the increase of V_g, the crossover shifts towards the anode and, at $V_g = 1.0 - 1.6$ kV, the beam is properly focused into the tunnel [Fig. 6(b)].

Note that at the edges of the beam there appear a ring-shaped domain, where the current density is much higher than in the center of the beam. As the grid voltage increases, the compression becomes weaker and this part of the beam begins to settle at the anode [Fig. 6(c)]. This results in rapid increase of the body current.

Fig. 7 demonstrates the electron current density profile in the midplane $x = 0$ calculated at $V_g = 1.48$ kV. At that voltage, the current of each beamlet is 62 mA that is almost two times higher than in the previous works [13] and [14]. Thus, the averaged current density at the cathode is 26.31 A/cm^2. Despite it is higher than the values reported in [12]–[14] where the cathode loading about 20 A/cm^2 was measured, it still seems available for the existing thermionic cathodes.

At the entrance of the beam tunnel, the beamlets have nearly elliptic shape with approximately 75 μm × 250 μm dimensions. Thus, one can estimate the compression factor as 16 and the averaged current density as $\sim$ 400 A/cm^2.

However, the current density distribution in the beam cross-section is essentially non-uniform that is typical for EOSs with high compression, see e.g. [12]. This is

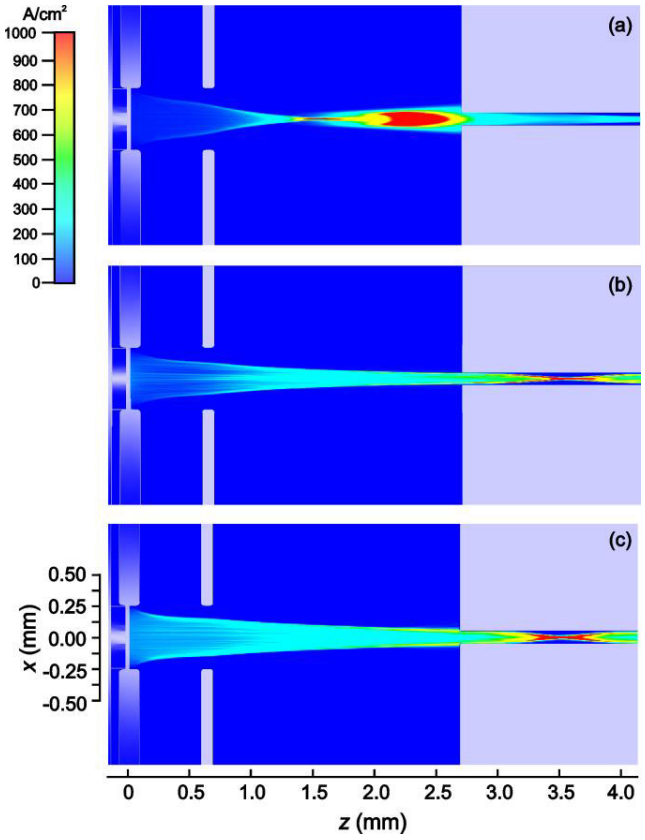

FIGURE 6. Electron beam current density profiles in the midplane $y = 0$ at $V_a = 21.4$ kV and $V_g = 0.5$ kV (a), 1.48 kV (b), and 1.7 kV (c).

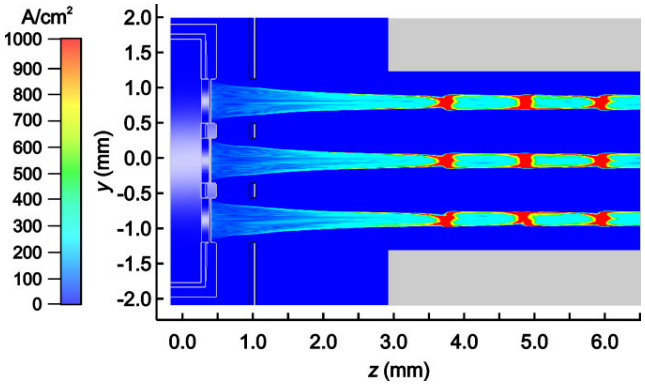

FIGURE 7. Electron beam current density profile in the midplane $x = 0$ at $V_g = 1.48$ kV and $V_a = 21.4$ kV.

demonstrated in Fig. 8 where current density profiles in x-y cross section at different distances from the cathode are plotted. The beam exhibits ripple, which is most pronounced in the vertical direction. In Fig. 8, one can see the abovementioned ring-shaped high-current-density domains at the edge of the beams. At the points of maximal compression, e.g., at $z = 4.8$ mm or at $z = 6.0$ mm, the current density attains very high values $\sim 10^3$ A/cm^2.

Fig. 9 illustrates the results of beam transportation inside the 0.1 mm $\times$ 2.4 mm beam tunnel. In this figure, electron beam profiles in x,z and y,z planes are plotted. This figure

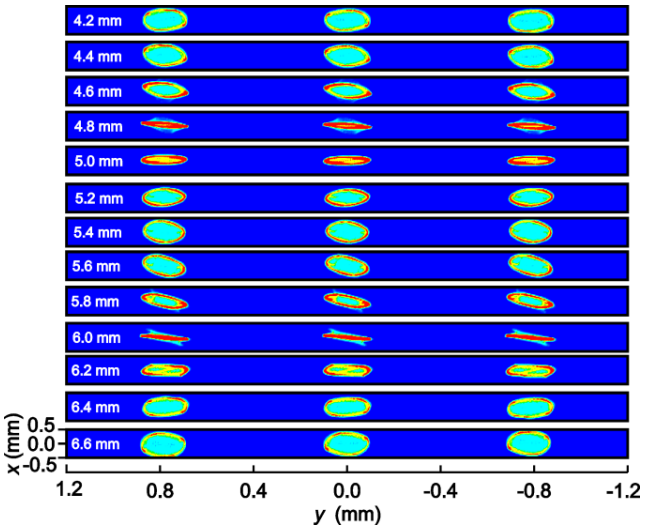

FIGURE 8. Electron beam current density profiles in x-y plane inside the beam tunnel at different distances from the cathode.

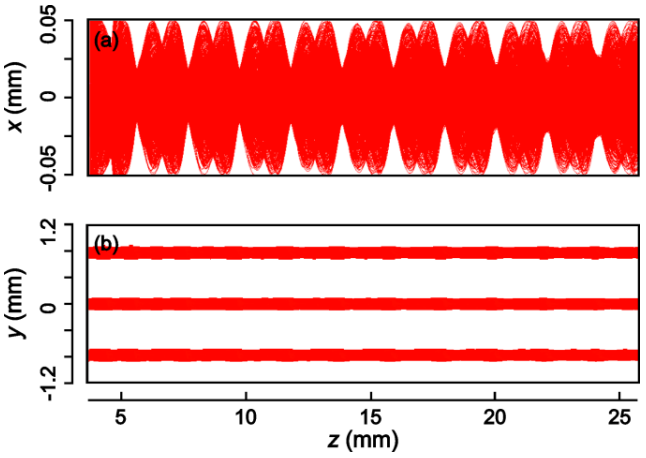

FIGURE 9. Electron beam transportation in the beam tunnel. (a) Side view in the x,z plane. (b) Top view in the y,z plane.

clearly demonstrates ripples with a spatial period determined by the cyclotron wavelength $\lambda_c = 2\pi v_{0z}/\omega_c \approx 2.4$ mm, where v_{0z} is the dc beam velocity and ω_c is the electron cyclotron frequency. However, Fig. 9(a) reveals a more complicated shape in the x,z plane, which is nearly bi-periodic. This shape is explained by the motion of the particles, which form the low-density halo of the beam (see [12] for details). These particles have high transversal velocities, which may reach 10% of the axial velocity. Fig. 9 shows stable propagation of the beam at nearly 25 mm distance that is sufficient for effective beam-wave interaction in a 0.2-THz TWT.

IV. CONCLUSION

In this article, we present the design of a novel multiple-beam EOS for a 0.2-THz TWT. This EOS provides formation of the triple elliptic beam for interaction with higher-order transversal mode of the overmoded SWS. The simulations predict 16-times compression of the beam. The cathode loading

is 26.31 A/cm^2 while the averaged current density in the beam tunnel exceeds 400 A/cm^2.

The triode electron gun with planar electrodes has been selected since such a design simplifies the fabrication process. The control grid voltage can be adjusted for effective beam focusing. The simulation demonstrates stable transportation of the 3 × 0.06 A beam at 25-mm distance in the 0.1 mm × 2.4 mm tunnel. These parameters are sufficient to provide high-gain, high-power operation of the 0.2-THz TWT with staggered grating SWS [20].

Fabrication and assembling of the gun is now in progress. The future research will be aimed at experimental measurements of current-voltage characteristics as well as at studies of the beam transmission.

REFERENCES

[1] G. S. Nusinovich, S. J. Cooke, M. Botton, and B. Levush, "Wave coupling in sheet- and multiple-beam traveling-wave tubes," *Phys. Plasmas*, vol. 16, no. 6, Jun. 2009, Art. no. 063102, doi: 10.1063/1.3143123.

[2] Y.-M. Shin, "Superimposed coherent terahertz wave radiation from mono-energetically bunched multi-beam," *Phys. Plasmas*, vol. 19, no. 6, Jun. 2012, Art. no. 063115, doi: 10.1063/1.4731695.

[3] A. Gee and Y.-M. Shin, "Gain analysis of higher-order-mode amplification in a dielectric-implanted multi-beam traveling wave structure," *Phys. Plasmas*, vol. 20, no. 7, Jul. 2013, Art. no. 073106, doi: 10.1063/1.4813800.

[4] C. Ruan, M. Zhang, J. Dai, C. Zhang, S. Wang, X. Yang, and J. Feng, "*W*-band multiple beam staggered double-vane traveling wave tube with broad band and high output power," *IEEE Trans. Plasma Sci.*, vol. 43, no. 7, pp. 2132–2139, Jul. 2015, doi: 10.1109/TPS.2015.2435160.

[5] G. Shu, G. Liu, L. Chen, H. Bambarandage, and Z. Qian, "Terahertz backward wave radiation from the interaction of high-order mode and double sheet electron beams," *J. Phys. D, Appl. Phys.*, vol. 51, no. 5, Feb. 2018, Art. no. 055107, doi: 10.1088/1361-6463/aaa20e.

[6] Z. Zhang, C. Ruan, A. K. Fahad, C. Zhang, Y. Su, P. Wang, and W. He, "Multiple-beam and double-mode staggered double vane travelling wave tube with ultra-wide band," *Sci. Rep.*, vol. 10, p. 20159, Nov. 2020, doi: 10.1038/s41598-020-77204-w.

[7] Z. Zhang, C. Ruan, W. Wang, and W. He, "Design and stability analysis of a high-order mode-staggered double vane traveling wave tube with two pencil beams at G-band," *IEEE Trans. Plasma Sci.*, vol. 49, no. 9, pp. 3029–3034, Sep. 2021, doi: 10.1109/TPS.2021.3100523.

[8] G. Shu, G. Liu, Z. Qian, and W. He, "Design, microfabrication, and characterization of a subterahertz-band high-order overmoded double-staggered grating waveguide for multiple-sheet electron beam devices," *IEEE Trans. Electron Devices*, vol. 68, no. 6, pp. 3021–3027, Jun. 2021, doi: 10.1109/TED.2021.3075417.

[9] Y. Zheng, D. Gamzina, B. Popovic, and N. C. Luhmann, "Electron beam transport system for 263-GHz sheet beam TWT," *IEEE Trans. Electron Devices*, vol. 63, no. 11, pp. 4466–4472, Nov. 2016, doi: 10.1109/TED.2016.2606322.

[10] S. Wang, S. Aditya, J. Miao, and X. Xia, "Design of a sheet-beam electron-optical system for a microfabricated *W*-band traveling-wave tube using a cold cathode," *IEEE Trans. Electron Devices*, vol. 63, no. 9, pp. 3725–3732, Sep. 2016, doi: 10.1109/TED.2016.2589285.

[11] L. Yang, J. Wang, H. Li, W. Jiang, K. Dong, and Y. Luo, "Study of a novel bidirectional compression electron gun for *W*-band sheet beam TWT," *IEEE Trans. Plasma Sci.*, vol. 45, no. 5, pp. 805–810, May 2017, doi: 10.1109/TPS.2017.2688480.

[12] I. A. Navrotsky, A. A. Burtsev, V. V. Emelyanov, V. N. Titov, and N. M. Ryskin, "Electron-optic system with a converged sheet electron beam for a 0.2-THz traveling-wave tube," *IEEE Trans. Electron Devices*, vol. 68, no. 2, pp. 798–803, Feb. 2021, doi: 10.1109/TED.2020.3041425.

[13] I. A. Navrotsky, A. A. Burtsev, A. Y. Kivokurtsev, K. V. Shumikhin, P. D. Shalaev, T. A. Karetnikova, and N. M. Ryskin, "Development of electron-optical system with three elliptic electron beams for a THz-band vacuum-tube device," in *Proc. 10th U.K.-Europe-China Workshop Millimetre Waves Terahertz Technol. (UCMMT)*, Liverpool, U.K., Sep. 2017, pp. 1–2, doi: 10.1109/UCMMT.2017.8068467.

[14] I. A. Navrotsky, A. A. Burtsev, A. V. Danilushkin, T. A. Karetnikova, N. M. Ryskin, and K. V. Shumikhin, "Developing of EOS model with elliptical beams for THz devices," in *Proc. Int. Conf. Actual Problems Electron Devices Eng. (APEDE)*, vol. 1, Sep. 2018, pp. 170–174, doi: 10.1109/APEDE.2018.8542203.

[15] W. Shao, D. Xu, Z. Wang, H. Gong, Z. Lu, Z. Duan, Y. Wei, Y. Gong, and S. Aditya, "Stacked dual beam electron optical system for THz integrated wideband traveling wave tube," *Phys. Plasmas*, vol. 26, no. 6, Jun. 2019, Art. no. 063106, doi: 10.1063/1.5096331.

[16] H. Liang, Q. Xue, C. Ruan, J. Feng, S. Wang, X. Liu, and Z. Zhang, "Integrated planar three-beam electron optics system for 220-GHz folded waveguide TWT," *IEEE Trans. Electron Devices*, vol. 65, no. 1, pp. 270–276, Jan. 2018, doi: 10.1109/TED.2017.2773835.

[17] C. Ruan, P. Wang, H. Zhang, Y. Su, J. Dai, Y. Ding, and Z. Zhang, "Design of planar distributed three beam electron gun with narrow beam separation for w band staggered double vane TWT," *Sci. Rep.*, vol. 11, no. 1, p. 940, Dec. 2021, doi: 10.1038/s41598-020-80276-3.

[18] P. Wang, Y. Su, Z. Zhang, W. Wang, and C. Ruan, "Planar distributed three-beam electron optics system with narrow beam separation for fundamental-mode TWT in W-band," *IEEE Trans. Electron Devices*, vol. 68, no. 10, pp. 5215–5219, Oct. 2021, doi: 10.1109/TED.2021.3105363.

[19] A. E. Ploskikh, and N. M. Ryskin, "Simulation of a sub-THz traveling wave tube with multiple sheet electron beam," *Izvestiya Saratov Univ. New: Phys.*, vol. 19, no. 2, pp. 113–121, 2019, doi: 10.18500/1817-3020-2019-19-2-113-121.

[20] N. M. Ryskin, G. V. Torgashov, R. A. Torgashov, A. E. Ploskih, A. G. Rozhnev, V. N. Titov, A. V. Starodubov, I. A. Navrotskiy, and V. V. Emelyanov, "Development of miniature millimeter-band traveling-wave tubes with sheet and multiple electron beams," in *Proc. 7th All-Russian Microw. Conf. (RMC)*, Moscow, Russia, Nov. 2020, pp. 94–97, doi: 10.1109/RMC50626.2020.9312288.

[21] *CST Studio Suite Electromagnetic Field Simulation Software*. Dassault Systemes Deutschland GmbH. Accessed: Dec. 2021. [Online]. Available: https://www.3ds.com/products-services/simulia/products/cst-studio-suite/

IGOR A. NAVROTSKY received the M.Sc. degree in applied mathematics from Saratov State University, Saratov, Russia, in 2011.

Since 2012, he has been with "Almaz" RPE, Saratov, where he is currently a Senior Researcher with the Fundamental Research Laboratory. Since 2017, he also has been with the Saratov Branch, Kotelnikov Institute of Radio Engineering and Electronics RAS. His research interests include electron-optic systems design and development and microfabrication of slow-wave structures for THz-band traveling-wave tubes.

NIKITA M. RYSKIN (Senior Member, IEEE) received the Diploma, Ph.D., and D.Sc. degrees from Saratov State University, Saratov, Russia, in 1991, 1996, and 2005, respectively.

Since 1991, he has been with Saratov State University, where he is currently a Professor and the Chair of the Department of Dynamical Systems. In 2013, he also joined Saratov Branch, Kotelnikov Institute of Radio Engineering and Electronics RAS, where he is also the Head of the Vacuum Micro- and Nanoelectronics Laboratory. He conducted research on time-domain simulation of nonlinear and chaotic phenomena in various vacuum microwave electron devices (BWO, TWT, and klystrons). He has coauthored more than 250 journal articles and conference papers, and two books. His current research interests include development of miniaturized sub-THz and THz vacuum tubes and theoretical study of nonlinear phenomena in gyrotron and other microwave oscillators.

Prof. Ryskin served as a member of the IEEE EDS Vacuum Electronics Technical Committee, from 2015 to 2018.